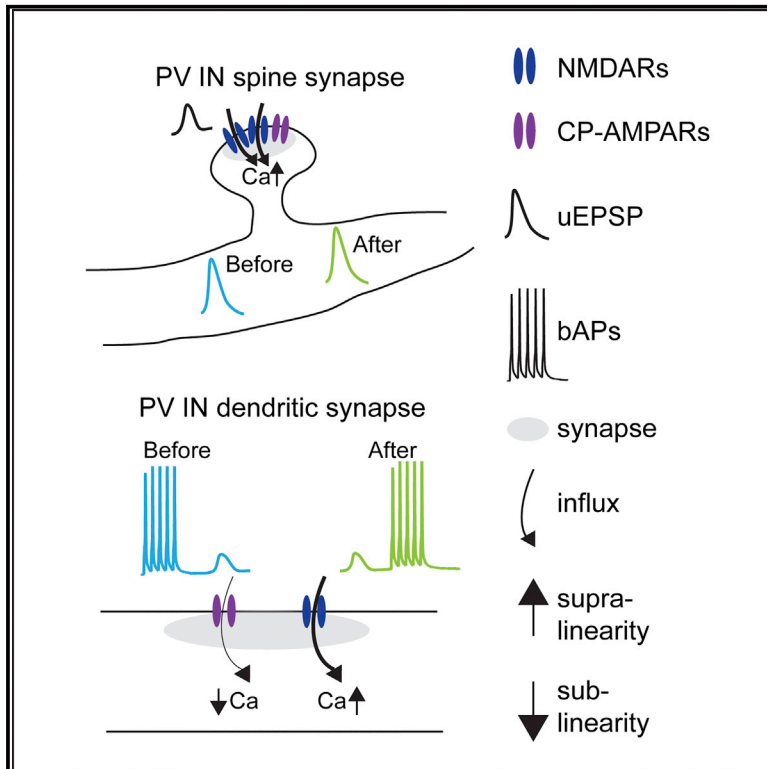


Functional Distinctions between Spine and Dendritic Synapses Made onto Parvalbumin-Positive Interneurons in Mouse Cortex

Graphical Abstract



Authors

Laura Sancho, Brenda L. Bloodgood

Correspondence

blbloodgood@ucsd.edu

In Brief

Sancho and Bloodgood demonstrate that in the mouse cortex, spines on PV interneurons contain glutamatergic synapses. Spine and dendritic synapses have CP-AMPA receptors and NMDARs, but spines are enriched for NMDARs. These synapses are functionally distinct. Dendritic synapses are modulated by action potentials, while spine synapses are sensitive to local activity.

Highlights

- Spines on PV INs contain glutamatergic synapses
- NMDARs are biased toward spine synapses
- Dendritic CP-AMPA receptors and NMDARs are bidirectionally modulated by somatic activity
- Local dendritic depolarization generates spine Ca supra-linearities via NMDARs



Functional Distinctions between Spine and Dendritic Synapses Made onto Parvalbumin-Positive Interneurons in Mouse Cortex

Laura Sancho^{1,2} and Brenda L. Bloodgood^{1,2,3,*}

¹Neurosciences Graduate Program, University of California, San Diego, 9500 Gilman Drive, La Jolla, CA 92093-0634, USA

²Division of Biological Sciences, Section of Neurobiology, Center for Neural Circuits and Behavior, University of California, San Diego, 9500 Gilman Drive, La Jolla, CA 92093-0634, USA

³Lead Contact

*Correspondence: bbloodgood@ucsd.edu

<https://doi.org/10.1016/j.celrep.2018.07.070>

SUMMARY

Dendritic spines influence synapse function by boosting synaptic potentials and sequestering synaptically generated second messengers. Spines have been extensively studied in densely spiny principal neurons, but little is known about how they expand the information-gathering capabilities of sparsely spiny interneurons (INs). We find in the mouse primary visual cortex, parvalbumin-positive INs have a low density of spines that enclose functional glutamatergic synapses. Both spine and dendritic synapses contain calcium-permeable AMPA receptors (CP-AMPA) and NMDA receptors (NMDARs), but NMDARs are enriched at spine synapses. Glutamate-receptor-mediated Ca influx at proximal dendritic sites is bidirectionally modulated by the timing of action potentials (APs). Surprisingly, spine synapses are largely insensitive to APs, but coincident activity originating in the adjacent dendrite strongly influences spine NMDAR-mediated calcium influx. Thus, while glutamate receptors on spines and dendrites are modulated by the activity of the neuron, they are distinctive in the type of coincident activity detected.

INTRODUCTION

Excitatory synapses are formed onto dendritic spines and directly onto the dendritic shaft. A synapse that is enclosed within a spine head can produce a local synaptic potential that is tens of millivolts in amplitude (Yuste, 2013; Jayant et al., 2017; Kwon et al., 2017), while a similar current originating from a dendritic shaft synapse may be an order of magnitude smaller (Gulledge et al., 2012; Kawato and Tsukahara, 1984; Araya et al., 2006). The large synaptic potentials produced at spine synapses can engage an array of local voltage-dependent receptors and channels (Bloodgood et al., 2009; Sabatini and Svoboda, 2000; Sobczyk et al., 2005; Bloodgood and Sabatini,

2007), which shape the amplitude and kinetics of synaptic calcium (Ca) signals. Thus, the signaling repertoire of a synapse is a function of both its physical location and the complement of receptors and channels present.

The consequences of housing a synapse within a spine have been extensively explored in densely spiny principal neurons (PNs), where the overwhelming majority of excitatory synapses are made onto spines. However, many inhibitory interneurons (INs) are sparsely spiny with spine densities that vary based on IN subtype (Peters and Regidor, 1981; Kawaguchi et al., 2006; Azouz et al., 1997). In INs where spines have been studied, these spines contain functional synapses and undergo experience-driven structural plasticity (Keck et al., 2011; Guirado et al., 2014; Pérez-Rando et al., 2017; Gilabert-Juan et al., 2011), as observed for spines on PNs. Nonetheless spine synapses are interspersed among and often outnumbered by those formed directly onto the dendrites, raising the question of how spine synapses expand the information gathering capabilities of sparsely spiny INs.

Parvalbumin-positive (PV) INs are a compelling cell type in which to study the operations performed by spine versus dendritic synapses. First, the dendrites of PV INs are densely innervated, receiving up to three excitatory synaptic inputs per micron (Gulyás et al., 1999). While this cell type is often described as having smooth dendrites, spines have been observed on the dendrites of PV INs in many brain regions, at various developmental stages, and in several species (Kawaguchi et al., 2006; Gulyás et al., 1999; Kubota et al., 2011). However, it has not been established whether spines on PV INs enclose synapses, let alone whether they are functionally distinct from synapses made onto the dendrites.

Second, excitatory synapses on PV INs contain both Ca-permeable AMPA receptors (CP-AMPA) and NMDA receptors (NMDARs) (Goldberg et al., 2003a; Geiger et al., 1997; Matta et al., 2013). Both of these receptor types are Ca permeable and highly voltage dependent (Kamboj et al., 1995; Nowak et al., 1984; Jonas et al., 1994) with inverse sensitivities to membrane potential. Thus, the versatility of synaptic Ca signaling executed by PV INs may be expanded by variability in the glutamate receptor composition of individual synapses in conjunction with whether or not the synapse is enclosed by a spine or made directly onto the dendrite.



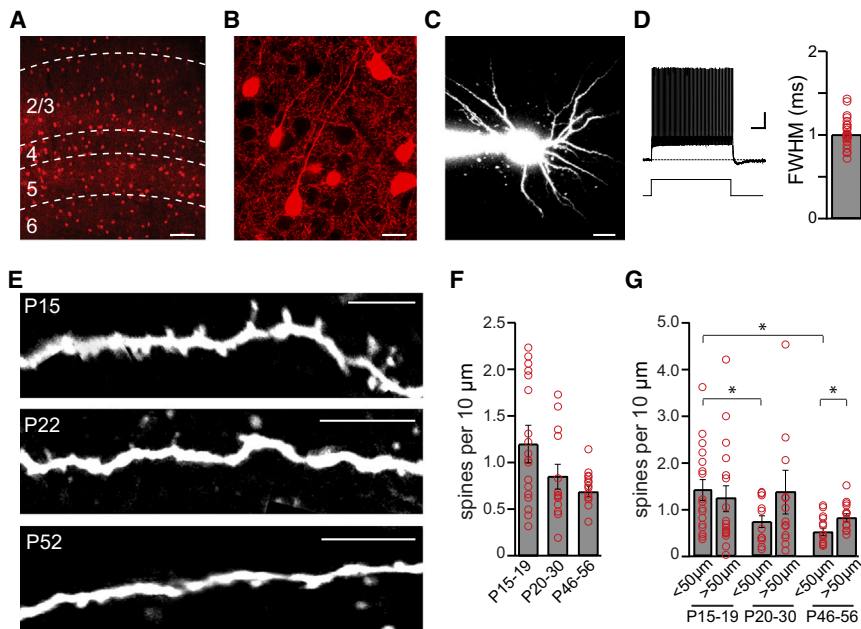


Figure 1. PV INs Are Sparsely Spiny

(A) Confocal image of V1 from a *Pvalb^{tm1(cre)Arbr} × Gt(ROSA)26Sor^{tm14(CAG-tdTomato)Hze}* mouse. Scale bar, 100 μ m. (B) Layer II/III PV INs in V1. Scale bar, 20 μ m. (C) Two-photon image of a tdTomato-expressing PV IN filled with Alexa Fluor-594. Scale bar, 20 μ m. (D) Left: representative trace in response to somatic current injection (1 s, 400 pA). Scale bars, 10 mV and 100 ms. Right: AP full width at half maximum (FWHM; n = 24 neurons, 16 mice). (E) PV IN dendrites. Scale bars, 10 μ m. (F) Spine density from P15 to P19 (n = 17 branches, 11 neurons, 6 mice), P20 to P30 (n = 13 branches, 10 neurons, 4 mice), and P46 to P56 (n = 13 branches, 6 neurons, 3 mice). p = 0.077, Kruskal-Wallis test. (G) Spine density in proximal (first 50 μ m) and distal (remaining length) dendrites. Proximal versus distal: P15–P19, p = 0.62; P20–P30, p = 0.15; P46–P56, p = 0.016 (Wilcoxon signed ranks test). Proximal versus proximal: p = 0.0040; P15–P19 versus P20–P30, p = 0.030; P15–P19 versus P46–56, p = 0.0070. Distal versus distal: p = 0.97. Kruskal-Wallis test for three-way comparisons, pairwise comparisons adjusted by Bonferroni correction. Red circles indicate individual branches. Data are shown as mean \pm SEM.

Finally, there is evidence that CP-AMPA and NMDARs are not uniformly distributed among all synapses made onto PV INs. In comparison to other cell types, the AMPAR to NMDAR current ratio is large in PV INs (Matta et al., 2013; Camiré and Topolnik, 2014; Nissen et al., 2010). In the hippocampus, only a subset of synapses is capable of expressing NMDAR-dependent plasticity (Le Roux et al., 2013). In the somatosensory cortex, glutamatergic transmission from thalamic afferents produces NMDAR currents (Bagnall et al., 2011), while in the visual cortex, this is not the case (Kloc and Maffei, 2014). However, dendritic synapses produce Ca signals that are an amalgamation of Ca influx through CP-AMPA and NMDARs (Goldberg et al., 2003a, 2003c). Thus, when categorically considering PV INs, NMDARs are expressed at low levels, yet are nevertheless functionally significant at subsets of synapses and absent from others. This led us to ask if NMDARs are biased to spine synapses on PV INs, where the biophysical properties of the spine may specifically enhance NMDAR signaling while minimizing Ca influx through CP-AMPA.

We find that in layer II/III of the mouse primary visual cortex (V1), spines on PV INs enclose functional glutamatergic synapses. Using two-photon glutamate uncaging in combination with electrophysiology, Ca imaging, and pharmacology, we find that CP-AMPA-mediated Ca signals are similar in spines and dendrites, while NMDAR-mediated Ca influx is larger in spines. Additionally, we find that dendritic glutamate receptors are bidirectionally modulated by the timing of coincident action potentials (APs), whereas spine synapses are insensitive to APs yet highly influenced by excitatory postsynaptic potentials (EPSPs) originating in the adjacent dendritic shaft. Together, these characteristics imbue dendritic and spine synapses with distinct sensitivities to the ongoing activity of the neuron.

RESULTS

PV INs in Layer II/III of V1 Are Sparsely Spiny

We quantified spine density in PV INs of *Pvalb^{tm1(cre)Arbr} × Gt(ROSA)26Sor^{tm14(CAG-tdTomato)Hze}* mice. Whole-cell recordings were obtained from tdTomato-expressing INs in layer II/III of V1 (Figures 1A–1C). AP and membrane properties were consistent with fast-spiking, PV-positive INs (Figure 1D; full width at half maximum [FWHM], 1.0 ± 0.04 ms; input resistance [R_{in}], 113.1 ± 9.3 M Ω ; membrane capacitance [C_m], 36.4 ± 2.0 pF; spike rate, 83.9 ± 6.2 Hz; Azouz et al., 1997). We detected approximately one spine per 10 μ m, and spine densities were similar in tissue from mice before, during, and after the critical period (Figure 1F; post-natal day 15 [P15] to P19: 1.2 ± 0.1 , P20–P30: 0.85 ± 0.1 , P45–P56: 0.69 ± 0.054 spines/10 μ m). In younger mice, spine density was comparable along the length of the dendrite (Figure 1G; P15–P19, <50 μ m: 1.4 ± 0.2 , >50 μ m: 1.2 ± 0.3 spines/10 μ m). With age, there was a significant decrease in the spine density on the proximal dendrites, while density on distal dendrites was stable (Figure 1G; P20–P30, <50 μ m: 0.7 ± 0.1 , >50 μ m: 1.4 ± 0.5 ; P46–P56, <50 μ m: 0.52 ± 0.083 , >50 μ m: 0.83 ± 0.085 spines/10 μ m). These data suggest that spines are a consistent yet dynamic anatomical feature of PV INs in the mouse visual cortex.

Spines on PV INs Enclose Functional Glutamatergic Synapses

Spine-like protrusions have been previously described in PV INs (Gulyás et al., 1999; Peters and Regidor, 1981), but it is unknown if these spines enclose functional synapses. Whole-cell voltage-clamp recordings were obtained from PV INs, and local axons were stimulated with an extracellular (EC)

electrode placed near a dendrite or spine (Figure 2A). At low stimulus intensities, an evoked excitatory postsynaptic current (EPSC) was recorded at the soma, but no Ca transient was detected locally (Figures 2C and 2G; see [Experimental Procedures](#)). The EC stimulus strength was gradually increased until an all-or-nothing Ca transient was observed in the dendrite or spine (Figures 2D, 2E, and 2H). In a fraction of trials for both dendritic and spine events, the stimulus failed to produce a Ca transient. This could be due to a failure in evoking an AP or of synaptic transmission, precluding the strict interpretation of failures as a reflection of release probability. Ca transients measured in spines had rapid rise times (20%–80%: 4.6 ± 0.6 ms), suggesting that they originated locally, and the evoked Ca transients were similar in amplitude and kinetics at dendrites and spines (Figure 2I).

To determine if the Ca transients were due to glutamatergic transmission and not direct depolarization of the membrane, NMDAR and AMPAR antagonists were sequentially applied to the bath (3-((R)-2-Carboxypiperazin-4-yl)-propyl-1-phosphonic acid [CPP] and 2,3-Dioxo-6-nitro-1,2,3,4-tetrahydrobenzo[f]quinoxaline-7-sulfonamide disodium salt [NBQX], respectively), and the evoked Ca transients were compared to control conditions. Blocking NMDARs significantly reduced the peak Ca transients in dendrites and spines; subsequent antagonism of AMPARs eliminated the remaining Ca signal (Figures 2J–2L). Thus, spines on PV INs contain functional glutamatergic synapses.

While CP-AMPA receptors contribute to dendritic synaptic Ca signals in PV INs (Goldberg et al., 2003a, 2003c), it is unknown if CP-AMPA receptors are also at spine synapses. Wash in of philanthotoxin-433 (PhTx) to block CP-AMPA receptors significantly reduced the evoked Ca transient at dendritic and spine synapses. The Ca signal was further reduced by the subsequent application of NBQX (Figures 2M–2O), leaving a small residual Ca transient, attributable to NMDARs. While evoked Ca transients measured at both dendrite and spine synapses are sensitive to NMDAR and CP-AMPA receptor blockers, the synapse-to-synapse variability was high, particularly for spine synapses (Figures 2L, 2O, and S1A). Thus, dendritic and spine synapses can contain both CP-AMPA receptors and NMDARs, but the glutamate receptor composition of individual synapses is variable, most notably for spines where synapses may lack either CP-AMPA receptors or NMDARs.

Two-Photon Glutamate Uncaging and Ca Imaging Reveals NMDARs Are Enriched at Spine Synapses

EC stimulation activates many synapses that are distributed throughout the neuron's dendrites, preventing concomitant analysis of synaptic potentials and Ca transients. In order to dissect the contributions of the two Ca-permeable glutamate receptor subtypes to the electrical and Ca signals produced by individual dendritic and spine synapses, we performed simultaneous two-photon 4-Methoxy-7-nitroindolyl (MNI)-glutamate uncaging and Ca imaging, in combination with electrophysiology and pharmacology, in both voltage and current clamp (Figure 3A; Bloodgood and Sabatini, 2007). Glutamate was uncaged at putative dendritic synapses, defined as current hotspots (Figures 3B and 3D), or at spine heads (Figures 3F and

S2A–S2D; see [Experimental Procedures](#)). Uncaging glutamate at dendritic hotspots resulted in Ca transients that were similar to those produced in response to EC stimulation (Figure 3C), indicating that uncaging at dendritic sites is comparable to synaptic transmission. Analogous experiments conducted in the presence of CPP resulted in uncaging-evoked EPSCs and EPSPs (uEPSC and uEPSP) that were similar to those measured in control experiments. However, the peak of the uEPSP-associated Ca transient was 26% smaller in CPP than in control conditions (Figures 3E and 3H–3K). Thus, NMDARs are activated by glutamate presented at discrete dendritic sites and contribute significantly to the resulting Ca signal, but not uEPSP.

Uncaging over spines produced uEPSCs that were similar to those produced at dendritic sites, although the uEPSPs were significantly smaller, and the corresponding Ca transients were larger (Figures 3F–3K). Repeating these experiments with NMDARs antagonized resulted in uEPSCs, uEPSPs, and uEPSP-evoked Ca transients that were nearly 50% smaller than in control experiments (Figures 3G–3I), with a notable reduction in the early and late phases of the uEPSC. The difference of the average uEPSC recorded in CPP from control conditions revealed a biphasic current consistent with early AMPAR-mediated boosting of NMDAR opening followed by the slower kinetics of NMDARs alone (Figure 3G; Lester et al., 1990; Bloodgood et al., 2009). It is unlikely that the difference in current amplitude in these two conditions results from differential activation of AMPARs, since glutamate uncaging was standardized by photobleaching and small-amplitude uEPSCs can produce large Ca transients in control conditions (Figure S2G). In stark contrast to dendrites, NMDARs at individual spines contribute significantly to both the depolarization and the associated Ca signal.

Is the larger contribution of NMDARs to signals originating from spines due to the biophysical properties of spines, or are there more NMDARs in spines than in dendrites? To evaluate receptor densities, NMDARs were pharmacologically isolated and the voltage dependence of the receptors eliminated by excluding magnesium (Mg) from the EC solution. Glutamate was uncaged at the spine head and then at multiple locations over the adjacent dendrite to get an average dendritic response (Figure 3L). With AMPARs blocked, it was not possible to identify putative dendritic synapses by uEPSC hotspots, but by sampling several locations, we were able to assess the general dendritic receptor density. Considering all nine spine-dendrite clusters, the uncaging-evoked Ca transient was 40% larger in the spine than in the dendrite (Figure 3M). Moreover, of the 31 individual dendritic sites probed, 29 produced a smaller Ca transient than the corresponding spine (Figure 3N). These data suggest spines have more NMDARs or NMDARs that flux more Ca than the neighboring dendrite (Monyer et al., 1992; Bloodgood and Sabatini, 2009).

CP-AMPA-Mediated Ca Influx and Depolarization Are Similar in Dendrites and Spines

To determine if CP-AMPA receptors are also unevenly distributed between dendrites and spines, we probed both locations in the presence of PhTx. Blockade of CP-AMPA receptors resulted in uEPSPs

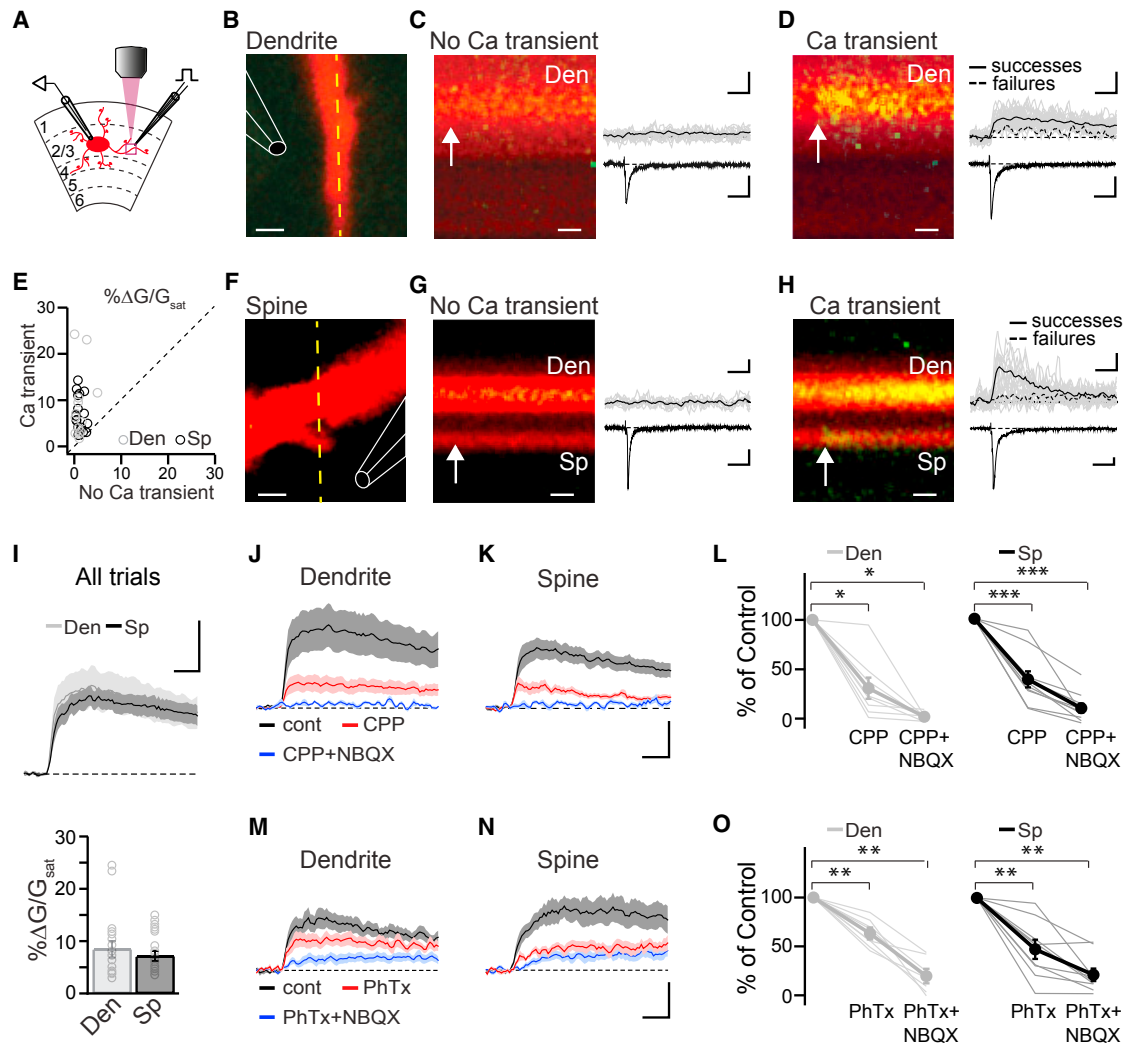


Figure 2. Spines on PV INs Enclose Functional Glutamatergic Synapses

(A) Schematic depicting a recording from a PV IN, the stimulating electrode, and two-photon Ca imaging.

(B) Representative dendritic segment. Dashed yellow line indicates line scans. Red, Alexa Fluor-594; green, Fluo-5F. Stimulating electrode is schematized in white. Scale bar, 1 μ m.

(C) Stimulation intensity evoking an EPSC but no Ca transient in the dendritic region of interest (ROI). Left: line scans through the dendrite in (B). Right: accompanying Ca transients ($n = 15$ trials; top). Ca transients: individual trials (gray) and mean (black). Bottom: average EPSC. Scale bars, 25 ms (left), 5% $\Delta G/G_{sat}$ and 50 pA (right).

(D) As in (C), but stimulation intensity evokes both an EPSC and a Ca transient in the ROI. $n = 25$ trials. Ca transients: individual trials (gray), mean of the successes (black), and mean of the failures (dashed). Scale bars, 25 ms (left), 5% $\Delta G/G_{sat}$ and 50 pA (right).

(E) $\Delta G/G_{sat}$ measured from “Ca transient” versus “no Ca transient.”

(F) As in (B), but for spines. Scale bar, 1 μ m.

(G) As in (C), but for spines. $n = 8$ trials. Scale bars, 25 ms (left), 10% $\Delta G/G_{sat}$ and 50 pA (right).

(H) As in (D), but for spines. $n = 23$ trials. Scale bars, 25 ms (left), 10% $\Delta G/G_{sat}$ and 50 pA (right).

(I) Population average of Ca transients. Top: average Ca transient including failures (number of trials: dendrites [Den] = 18 ± 2 , spines [Sp] = 23 ± 2 ; number of successes: dendrites = 13 ± 2 , spines = 15 ± 1). Scale bars, 5% $\Delta G/G_{sat}$ and 25 ms. Bottom: Ca peak including failures; individual cells: open gray circles. Dendrites = 8.8 ± 1.7 ($n = 17$, 9 mice), spines = 7.1 ± 9.3 ($n = 19$, 9 mice); $p = 0.79$. Successes only (not shown): dendrites = 10.9 ± 1.9 , spines = 10.5 ± 1.9 .

(J) Evoked Ca transients measured at dendritic hotspots in control conditions (cont; 10.8 ± 3.0) followed by wash-in of CPP (3.5 ± 1.2) and NBQX (0.2 ± 0.1 ; $n = 8$ dendrites, 8 neurons, 6 mice).

(K) As in (J) but in spines. Control = 8.0 ± 1.4 ; CPP = 3.1 ± 0.8 ; CPP + NBQX = 0.5 ± 0.2 ($n = 10$ spines, 10 neurons, 7 mice). Scale bars: 5% $\Delta G/G_{sat}$ and 25 ms.

(L) Ca peak as a percent of control with sequential wash-in of CPP and NBQX. Individual sites, thin lines; average, thick lines. p values for dendrite and spine. Control versus CPP: $p = 0.012/0.0093$. Control versus CPP + NBQX: $p = 0.012/0.0051$.

(M) Evoked Ca transients measured at dendritic hotspots in control conditions (7.0 ± 1.4) followed by wash-in of PhTx (4.2 ± 1.0) and NBQX (1.4 ± 0.5 ; $n = 9$ dendrites, 9 neurons, 3 mice).

(legend continued on next page)

and associated Ca transients that were significantly smaller than those measured in control experiments, and the magnitude of the decrease was comparable at dendritic sites and spines (Figures 4A and 4C–4E). This suggests that in contrast to NMDARs, CP-AMPA receptors have similar distributions between dendrites and spines.

Rectification of CP-AMPA Receptors Is Similar in Dendrites and Spines

Depolarization drives intracellular polyamines into the pore of CP-AMPA receptors (Geiger et al., 1995; Kamboj et al., 1995; Bowie and Mayer, 1995), resulting in an inward rectification of CP-AMPA receptor-mediated currents. As the biophysical properties of spines allow small currents to produce relatively large local depolarizations, we sought to determine if CP-AMPA receptors at spine synapses are susceptible to polyamine block during uEPSPs. Whole-cell recordings were made from PV INs with an internal solution lacking spermine, and intracellular polyamines were dialyzed out of the cell. In the absence of polyamines, uEPSPs and Ca signals were similar to those measured in control experiments for both dendrites and spines (Figures 4B–4E). Thus, it is unlikely that depolarization originating from individual spine or dendritic synapses is sufficient to engage the polyamine block of CP-AMPA receptors.

The affinity of polyamines for CP-AMPA receptors, and consequently the rectification of AMPA receptor-mediated currents, is also influenced by the receptor subunit composition (Washburn et al., 1997) and association with specific transmembrane AMPA receptor regulatory proteins (TARPs), such as stargazin, which is expressed in PV INs (Soto et al., 2007; Pelkey et al., 2015). Rectification curves obtained by uncaging at dendritic and spine sites (Figure S3) showed no difference in the rectification index (RI; Figure 4F). The current-voltage relationship for dendritic sites was near linear when spermine was excluded from the intracellular solution, confirming that rectification was due to polyamines. Thus, AMPA receptors at both locations have similar affinities for polyamines and are unlikely to be systematically different in composition or TARP interaction.

Ca Signaling Through Glutamate Receptors on Dendrites, but Not Spines, Is Bidirectionally Modulated by Back-Propagating APs

In PNs, NMDAR-mediated Ca signals are enhanced when an EPSP is paired with back-propagating action potentials (bAPs) (Nevian and Sakmann, 2006; Yuste and Denk, 1995; Magee and Johnston, 1997), and the precise timing of bAPs can lead to synaptic potentiation or depression (Markram et al., 1997; Froemke and Dan, 2002). While the dendrites of PV INs do not support the active back propagation of APs (Hu et al., 2010; Goldberg et al., 2003b), the proximal dendrites do depolarize tens of millivolts as the AP invades (Hu et al., 2010). Moreover, bAP-triggered Ca transients can be measured

in proximal dendrites and spines (Figures 5A–5D; Goldberg et al., 2003b) and are equivalent in both compartments. Since excitatory synapses made on PV INs contain both CP-AMPA receptors and NMDARs, it is unclear if bAPs would reduce or enhance synaptic Ca signals.

To examine the effects of pairing synaptic activation with bAPs, glutamate was uncaged at dendritic sites or spines within 50 μ m of the soma in conjunction with a burst of five somatically evoked bAPs that came either 10 ms before or after uncaging (Figure 5E; see Experimental Procedures), timing intervals that are optimal for spike-timing-dependent plasticity in PNs (Froemke and Dan, 2002). The impact on uncaging-evoked Ca transients was calculated as a nonlinearity index (NI; Figure 5E; see Experimental Procedures). Uncaging at dendritic sites resulted in Ca transients that were sub-linear when preceded by a burst of bAPs (NI_{before}) and supra-linear when the uEPSP was followed by bAPs (NI_{after} ; Figures 5F and 5G). Nearly all of the dendritic sites showed consistent bidirectional modulation of the uncaging-evoked Ca transient (Figure 5H), and NIs were not correlated with the amplitude of the Ca transient, indicating that sub-linearities were not due to saturation of the indicator (Figure S4). Reducing the latency between the dendritic uEPSP and bAPs to 2 ms selectively eliminated the sub-linearity when bAPs preceded the uEPSP (Figure 5H), suggesting that this sub-linearity is particularly timing dependent. Thus, proximal dendritic sites are sensitive to the relative timing of the PV IN's firing.

To test the dependence of the modulation of the uncaging-evoked Ca transient on different receptors, we repeated the above experiments in the presence of CPP or PhTx and focused on the 10-ms pairing condition as both sub- and supra-linearities were detected with this timing interval. Antagonizing NMDARs selectively eliminated the supra-linearity observed when bAPs followed the uEPSP (Figure 5I); blocking CP-AMPA receptors or omitting polyamines from the intracellular solution selectively abolished the sub-linearity observed when the bAPs preceded the uEPSP (Figures 5J and 5K). Thus, at dendritic sites, when spikes precede a uEPSP, synaptic Ca influx is reduced via modulation of CP-AMPA receptors, and when spikes follow a uEPSP, NMDAR-mediated Ca transients are enhanced.

Since spines have more NMDARs than dendrites, we hypothesized that spine synapses may be more sensitive to bAPs. Unexpectedly, when bAPs were paired with spine uEPSPs, neither timing resulted in a significant nonlinearity (Figures 6A–6C). Moreover, while the difference between when bAPs came before or after the uEPSP was significant, it was substantially smaller than that observed when uncaging at dendritic sites (dendrites, 31%; spines, 12%). Reducing the latency to 2 ms (Figure 6C), antagonizing NMDARs, or blocking CP-AMPA receptors did not reveal any significant changes in NIs (Figures 6D and 6E). In all conditions, the NI was uncorrelated with the amplitude of the Ca signal, again indicating these measurements are not obscured

(N) As in (M), but in spines. Control = 6.5 ± 1.2 ; PhTx = 2.2 ± 0.4 ; PhTx + NBQX = 1.2 ± 0.4 ($n = 9$ spines, 9 neurons, 2 mice). Scale bars, 5% $\Delta G/G_{\text{sat}}$ and 25 ms.

(O) As in (L), but with PhTx and NBQX. p values for dendrite and spine. Control versus PhTx: $p = 0.0077/0.0077$. Control versus PhTx + NBQX: $p = 0.0077/0.0077$. Data are shown as mean \pm SEM. A Mann-Whitney U test was used for unpaired data and Wilcoxon signed ranks test for paired data.

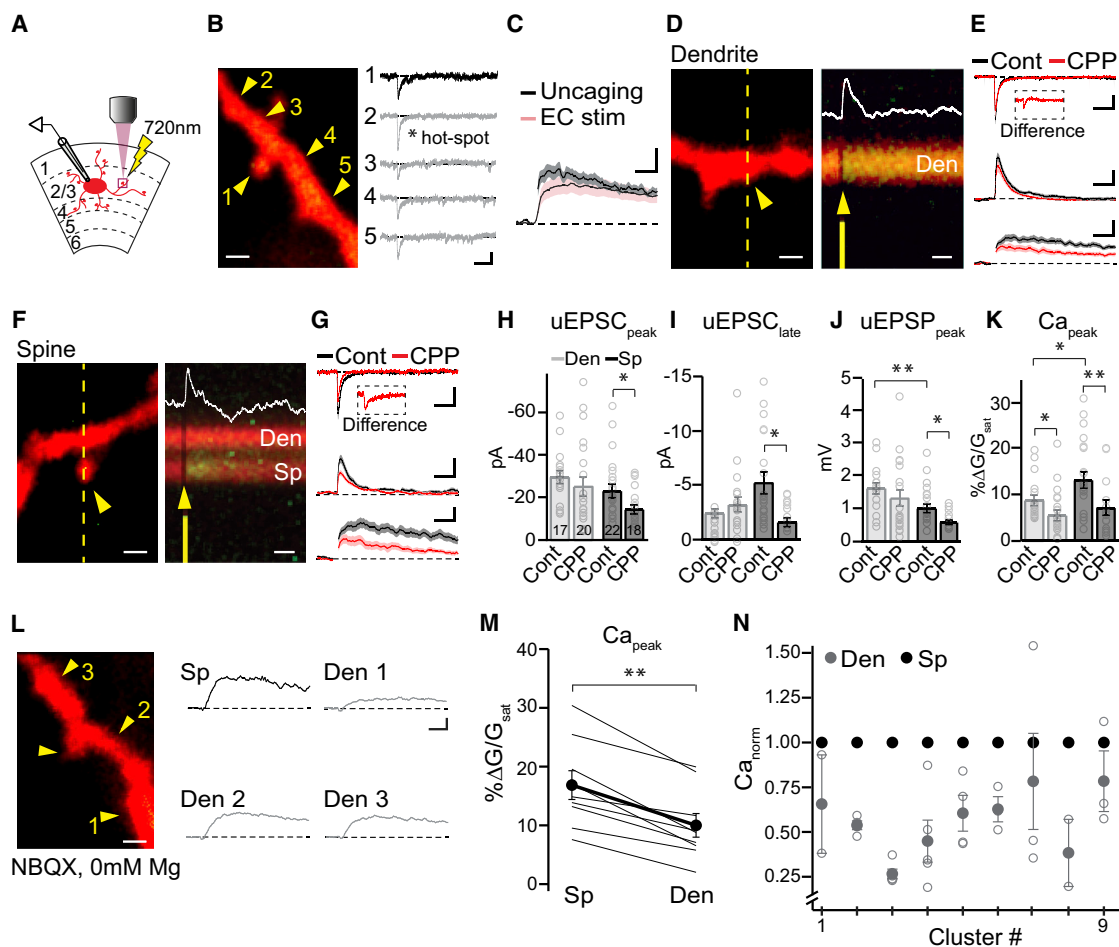


Figure 3. Spines Are Enriched for NMDARs

(A) Schematic depicting a recording from a PV IN, two-photon glutamate uncaging, and Ca imaging.

(B) Hotspot localization in dendritic shafts. Left: (1) uncaging power set at spine head, and (2–5) uncaging at multiple dendritic sites. Right: uEPSCs in response to uncaging at the corresponding sites. Scale bars, 1 μ m (left), 10 pA and 25 ms (right).

(C) Dendritic Ca transient in voltage clamp in response to uEPSCs and to EC stimulation. Scale bars, 5% Δ G/G_{sat} and 25 ms.

(D) Uncaging-elicited dendritic responses. Left: representative dendritic segment. Right: line scans through the region indicated by the dashed yellow line with example uEPSP inset in white. Yellow arrowhead indicates the location (left) or time (right) of the uncaging pulse. Scale bars, 1 μ m (left) and 25 ms (right).

(E) Dendritic population average: uEPSC (top), uEPSP (middle), and Ca transient (bottom) in control conditions (cont, n = 17 sites, 11 neurons, 9 mice) or in CPP (n = 20 sites, 10 neurons, 8 mice). Inset in the top panel is the uEPSC difference (control - CPP). Scale bars, 10 pA (top), 0.5 mV (middle), 5% Δ G/G_{sat} (bottom), and 25 ms.

(F) As described in (D), but with uncaging at a spine.

(G) As described in (E), but for spine population averages. Control conditions (n = 22 spines, 17 neurons, 16 mice) and CPP (n = 18 spines, 13 neurons, 9 mice).

(H–K) Responses to uncaging over dendrites and spines for control and CPP conditions. Open gray circles denote individual dendrites and spines. (H) Average uEPSC_{peak}. Dendrites: cont = -29.4 ± 3.0 , CPP = -25.3 ± 4.5 ; p = 0.18. Spines: cont = -23.6 ± 3.2 , CPP = -14.4 ± 2.1 ; p = 0.035. Dendrite versus spine, cont; p = 0.080. (I) uEPSC_{late}. Dendrites: cont = -2.4 ± 0.4 , CPP = -3.3 ± 0.7 ; p = 0.43. Spines: cont = -5.4 ± 1.1 , CPP = -1.6 ± 0.4 ; p = 0.011. Dendrite versus spine, cont; p = 0.11. (J) uEPSP_{peak}. Dendrites: cont = 1.6 ± 0.2 , CPP = 1.3 ± 0.3 ; p = 0.13. Spines: cont = 1.0 ± 0.1 , CPP = 0.6 ± 0.07 ; p = 0.022. Dendrite versus spine, cont; p = 0.0083. (K) Ca_{peak}. Dendrites: cont = 8.8 ± 1.1 , CPP = 5.6 ± 1.1 ; p = 0.014. Spines: cont = 13.9 ± 1.9 , CPP = 7.3 ± 1.7 ; p = 0.0088. Dendrite versus spine, cont; p = 0.023.

(L) Left, image of a spine and dendrite. Yellow arrowheads indicate uncaging sites. Right, uncaging-evoked Ca transients in the spine (spine) or each of three dendritic sites (dendrite 1–3). Scale bars, 1 μ m (left), 10% Δ G/G_{sat} and 25 ms (right).

(M) Ca_{peak} measured in the spine and average of the adjacent dendrite (dendrite, average of 2–4 sites). Individual spine/dendrite comparisons, thin lines; average, thick lines (n = 9 clusters, 6 neurons, 5 mice). Spine: $16.8 \pm 2.5\%$ Δ G/G_{sat}, dendrite: $10.0 \pm 2.5\%$ Δ G/G_{sat}; p = 0.0051.

(N) Comparison of spine and dendritic Ca normalized to the spine Ca_{peak} (cluster average, filled gray circle; individual site, open gray circle).

Data are shown as mean \pm SEM unless otherwise indicated. A Mann-Whitney U test was used for unpaired data and Wilcoxon signed ranks test for paired data.

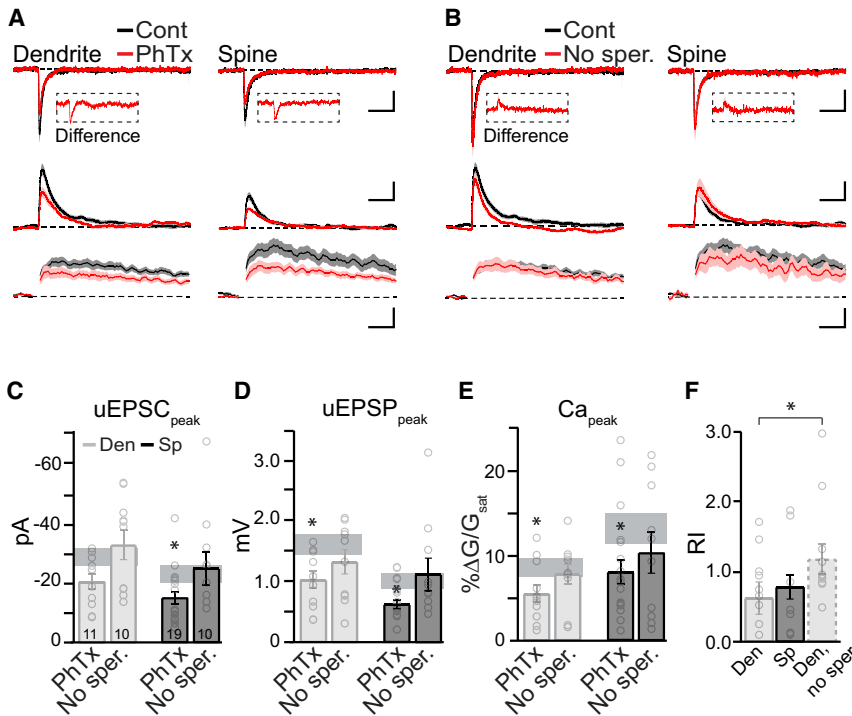


Figure 4. CP-AMPA-Mediated Ca Influx and Depolarization Are Similar in Dendrites and Spines

(A) Population average uEPSC (top), uEPSP (middle), and Ca (bottom) measured in response to uncaging at dendritic sites (left) or spines (right) in control conditions (replotted from Figure 3) or in PhTx (dendrite: $n = 11$ sites, 8 neurons, 5 mice; spine: $n = 19$ spines, 11 neurons, 8 mice). Inset in the top panel is the uEPSC difference. Scale bars, 10 pA and 25 ms (top), 0.5 mV and 25 ms (middle), and 5% $\Delta G/G_{\text{sat}}$ and 25 ms (bottom).

(B) As described in (A), but with no spermine in the patch pipette (dendrite: $n = 10$ sites, 5 neurons, 4 mice; spine: $n = 10$ spines, 5 neurons, 2 mice). Scale bars, 10 pA and 25 ms (top), 0.5 mV and 25 ms (middle), and 5% $\Delta G/G_{\text{sat}}$ and 25 ms (bottom).

(C–E) Average uncaging responses in (A) and (B). Open circles denote individual dendrites and spines. Horizontal shaded area indicates SEM range from control conditions. Comparisons against control experiments in Figure 3. (C) Average uEPSC_{peak}. Dendrites: PhTx = -21.0 ± 2.6 , $p = 0.057$; no spermine (sper.) = -33.5 ± 5.0 , $p = 0.29$. Spines: PhTx = -15.3 ± 2.1 , $p = 0.029$; no spermine = -25.4 ± 5.8 , $p = 0.89$. (D) uEPSP_{peak}. Dendrites: PhTx = 1.0 ± 0.2 , $p = 0.020$; no spermine = 1.3 ± 0.2 , $p = 0.55$. Spines: PhTx = 0.6 ± 0.07 , $p = 0.018$; no spermine = 1.1 ± 0.3 , $p = 1.0$.

(E) Ca_{peak}. Dendrites: PhTx = 5.7 ± 1.0 , $p = 0.046$; no spermine = 8.0 ± 1.2 , $p = 0.62$. Spines: PhTx = 8.3 ± 1.4 , $p = 0.025$; no spermine = 10.6 ± 2.5 , $p = 0.33$. (F) Average RIs for dendritic and spine uEPSCs. Dendrites: RI = 0.63 ± 0.23 ($n = 9$, 9 neurons, 4 mice), spines: RI = 0.78 ± 0.17 ($n = 9$, 9 neurons, 4 mice); $p = 0.44$. Dendrites, no spermine: RI = 1.2 ± 0.21 ($n = 11$, 11 neurons, 5 mice), $p = 0.025$ (versus dendrites).

Data are shown as mean \pm SEM. Mann-Whitney U tests were used.

by saturation of the indicator (Figure S5). Thus, proximal spine synapses, unlike their dendritic counterparts, are largely insensitive to somatic activity.

Spine Synapses Are Sensitive to the Co-activation of Neighboring Dendritic Synapses

If spine synapses are insensitive to bAPs, are they sensitive to EPSPs originating in the adjacent dendrite? Glutamate was uncaged at an individual spine alone or in combination with five uncaging pulses delivered at a nearby dendritic site, mimicking the depolarization that would be produced by a barrage of synaptic inputs (Figure 7A). Dendritic uncaging occurred either 2 ms before or after spine stimulation, timing intervals that are efficacious in PNs (Losonczy and Magee, 2006; Branco and Häusser, 2011), and nonlinearities in the spine Ca signal were calculated (Figure 7B; see Experimental Procedures). We observed that spine Ca signals were enhanced by dendritic uEPSPs, regardless of whether the dendritic uEPSPs preceded or followed the spine uEPSP (Figures 7C–7E), and the NIs were not correlated with the amplitude of the Ca signal (Figure S6A). While the dendritic uEPSPs resulted in supra-linear Ca influx, the uEPSPs summated linearly (Figure S6D). Moreover, comparing the magnitude of the paired uEPSP with the NI of the Ca signal revealed a strong positive correlation (Figure 7F). These data indicate that the supra-linearity in the Ca signal is mediated by a voltage-dependent mechanism.

The enhancement of Ca influx through NMDARs may underlie the supra-linearity measured. We repeated the above experiment with NMDARs antagonized and found that the spine Ca transients were no longer boosted by the dendritic uEPSP (Figures 7G and 7H). In contrast to control conditions, the NI was negatively correlated with uEPSP amplitude, possibly due to larger uEPSPs reducing the driving force through AMPARs leading to a Ca sub-linearity (Figure 7I). Reinforcing this idea, the uEPSPs summated sub-linearly with NMDARs blocked in both timing paradigms (Figure S6E). Finally, we repeated these experiments in voltage clamp and saw no significant nonlinearities (Figures 7J–7L and S6F), as expected for the voltage-dependent relief of Mg block of NMDARs. Thus, NMDARs at spine synapses, while insensitive to bAPs, are highly modulated by local dendritic depolarization.

DISCUSSION

Spines on PV INs Enclose Functional Glutamatergic Synapses Enriched with NMDARs

Little is known about how spines expand the information gathering capabilities of synapses on sparsely spiny INs. Our findings demonstrate that the dendrites of PV INs, while often described as smooth, have ~ 1 spine per 10 μm and that these spines enclose functional glutamatergic synapses. Spines have comparable CP-AMPA receptors but are enriched for NMDARs in comparison to dendritic sites. The similarities and distinctions between spine

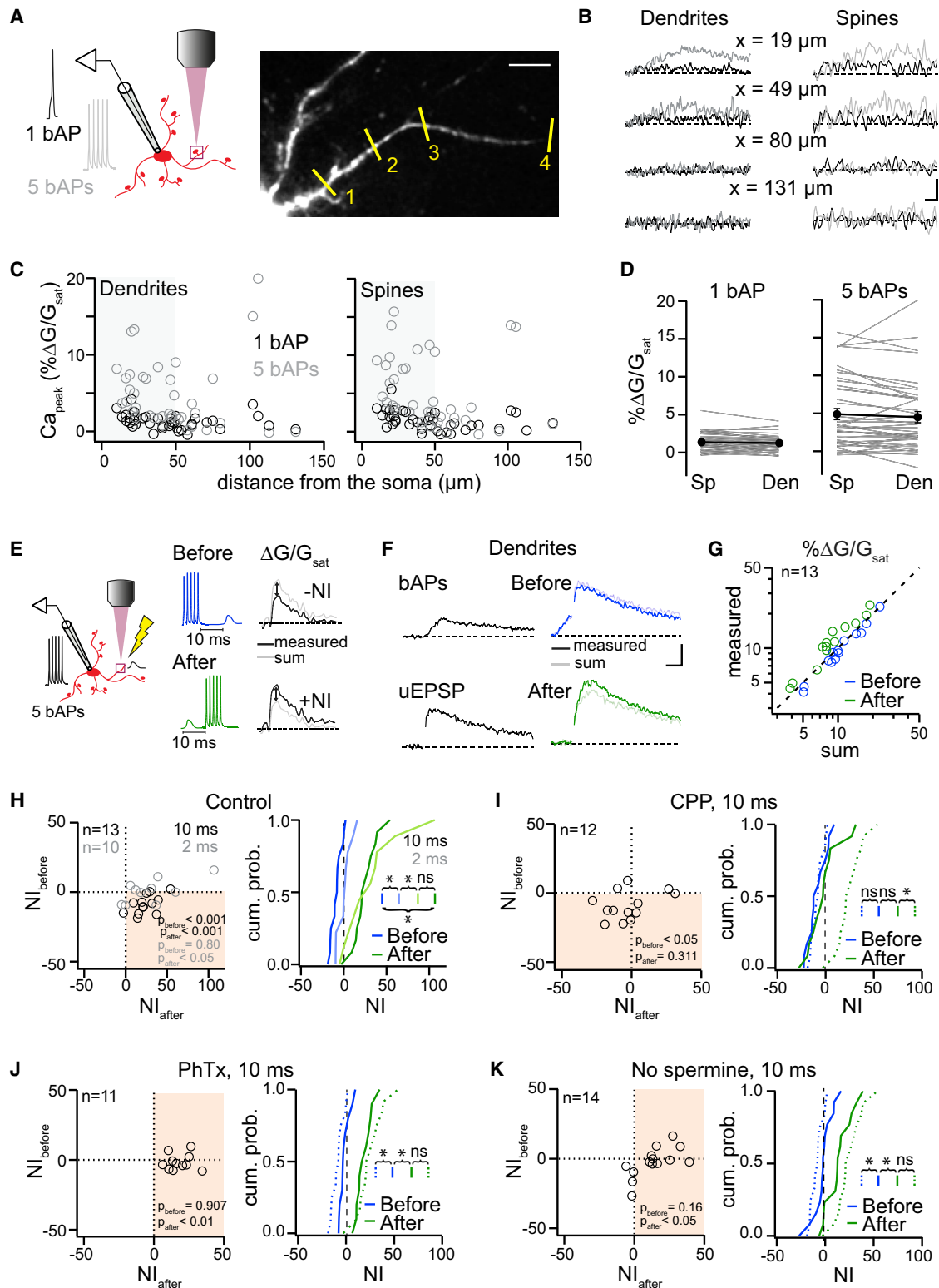


Figure 5. Ca Signaling through Glutamate Receptors on Dendrites Is Bidirectionally Modulated by bAPs

(A) Left: schematic showing 1 or 5 bAPs elicited by somatic current injection with simultaneous Ca imaging in the dendrite and spine. Right: Z stack of a PV IN dendrite. Yellow lines (1–4) indicate approximate regions imaged. Scale bar, 20 μm .

(legend continued on next page)

and dendritic synapses allude to receptor trafficking or turnover mechanisms that discriminate between these two compartments, perhaps through differential handling of receptors with a particular subunit composition, the selective sequestration or stabilization of NMDARs at spine synapses, or the removal and degradation of NMDARs in the dendrites.

Differences in the Modulation of Synaptic Ca by bAPs

We found that Ca influx at proximal dendritic sites is bidirectionally modulated by the coincident spiking of the neuron, indicating that dendritic synapses are highly sensitive to the neuron's integrated activity. Moreover, bAPs enhance or suppress synaptic Ca influx through modulation of NMDARs and CP-AMPA receptors, respectively. Thus, dendritic synapses on PV INs may use the relative timing of spikes to variably engage NMDAR- and CP-AMPA-dependent signaling pathways, providing a platform for triggering different forms of plasticity at these synapses.

We were surprised to see that bAPs had minimal impact on glutamate-receptor-mediated Ca influx at spine synapses, since bAPs readily invade spines and the biophysical properties of spines have been shown to boost synaptic depolarization and engage voltage-dependent receptors and channels. Perhaps spines are enriched for voltage-gated potassium channels that counteract bAP depolarization of the spine head, akin to their role in reducing back propagation in general (Hu et al., 2010). Irrespective of the mechanism, in our analysis spine synapses are insensitive to bAPs. Thus, it is unlikely that they are capable of undergoing plasticity that is coordinated with the output of the neuron, perhaps underlying the age-dependent loss of proximal spines.

Spines Are Sensors of Local Activity

While spine synapses are relatively insensitive to bAPs, their NMDARs are highly sensitive to depolarization that originates in the parent dendrite. This suggests spine synapses may engage NMDAR-dependent signaling pathways as synaptic ac-

tivity in the adjacent dendrite increases. It is also interesting to consider the density of spines on PV IN dendrites, as this may reflect the distance over which spine synapses sample dendritic activity (Lee et al., 2016) or signaling molecules that originate from spines exert their influence (Murakoshi et al., 2011; Nishiyama and Yasuda, 2015; Colgan and Yasuda, 2014). Moreover, this distance may be dynamically regulated by active conductances in the dendrites, such as Kv3.1 channels, which have been shown to modulate the spatial and temporal window of EPSP summation in PV INs (Hu et al., 2010).

Synaptic Plasticity in PV INs

We find that the location of a synapse, the specific receptor composition, and the timing and type of coincident activity all contribute to the repertoire of Ca signals produced by a synapse on a PV IN. Contextualizing these results, previous work has shown that both NMDARs and CP-AMPA receptors can induce long-term plasticity (Le Roux et al., 2013; Lamsa et al., 2007; Szabo et al., 2012), albeit with different induction protocols. Additionally, Ca nonlinearities, measured in the dendrites and produced by the activation of many synapses, can switch the direction of plasticity (Camiré and Topolnik, 2014). Furthermore, synaptic Ca signals are highly compartmentalized, either by the spine, receptor kinetics, or the precise localization of Ca pumps in the dendrites (Goldberg et al., 2003a), creating boundaries that can impose synapse-specific plasticity. It will be interesting to determine if spine synapses readily express NMDAR-mediated plasticity, while those formed on the dendrites may be subject to an ongoing competition between CP-AMPA and NMDAR-initiated signaling pathways. The identification of the presynaptic neurons that synapse on spines or will be likewise illuminating for our understanding of the specific operations performed by spine and dendritic synapses.

Role of NMDARs in Regulating PV IN Function

NMDARs are expressed at low levels in PV INs in comparison to other INs and PNs (Matta et al., 2013) yet are essential for PV IN

- (B) Ca transient measured at spine and adjacent dendrite indicated in (A) in response to 1 (black) or 5 bAPs (gray). Scale bars, 5% $\Delta G/G_{\text{sat}}$ and 50 ms.
- (C) bAPs evoked Ca transients plotted against distance from soma for dendrites (left) and spines (right). 1 bAP, black; 5 bAPs, gray ($n = 40$ sites, 14 neurons, 11 mice).
- (D) Ca peak measured for 1 bAP (left; spine versus dendrite, $p = 0.98$) or 5 bAPs (right; $p = 0.70$) in the spine compared to the adjacent dendrite. Mean \pm SEM are shown in black.
- (E) Left: schematic depicting the experimental setup. Middle: 5 bAPs (100 Hz) were evoked 10 ms before or after uncaging over the dendrite. Right: schematic of example nonlinearity indexes (NIs).
- (F) Average Ca transients measured from the dendrite in response to 5 bAPs (3.0 ± 0.8) or uncaging at the dendrite alone (7.0 ± 1.2) and in before and after (before = 10.6 ± 1.4 , after = 12.1 ± 1.6) pairing configurations. Scale bars, 5% $\Delta G/G_{\text{sat}}$ and 50 ms.
- (G) Measured versus sum of the Ca transients produced by bAPs and uEPSP alone ($n = 13$, 9 neurons, 4 mice).
- (H) Control, 10 ms (black) and 2 ms (gray). Left: NIs for each dendritic site (10 ms: $n = 13$, 9 neurons, 4 mice; 2 ms: $n = 10$, 6 neurons, 3 mice). 10 ms, $NI_{\text{before}} = -8.8\% \pm 1.8\%$ ($p = 8.6E-04$), $NI_{\text{after}} = 24.0\% \pm 4.0\%$ ($p = 0.00014$); 2 ms, $NI_{\text{before}} = 0.7\% \pm 2.7\%$ ($p = 0.80$); $NI_{\text{after}} = 30.2 \pm 10.6$ ($p = 0.013$; Wilcoxon signed ranks test, measured versus sum). Right: cumulative probability distributions of the NIs. 10 ms: NI_{before} versus NI_{after} , $p = 4.5E-07$; 2 ms: NI_{before} versus NI_{after} , $p = 0.0096$. 10 ms versus 2 ms: NI_{before} , $p = 0.010$; NI_{after} , $p = 0.59$.
- (I–K) Within-condition comparisons done as in (G). Between-condition comparisons done against control, 10 ms data (dotted lines).
- (I) CPP, 10 ms ($n = 12$, 8 neurons, 4 mice). Left: $NI_{\text{before}} = -9.0\% \pm 2.8\%$, $p = 0.023$; $NI_{\text{after}} = -2.4\% \pm 4.7\%$, $p = 0.31$ (Wilcoxon signed ranks test). Right: NI_{before} versus NI_{after} , $p = 0.17$. NI_{before} , $p = 0.95$; NI_{after} , $p = 0.00026$.
- (J) PhTx, 10 ms ($n = 11$, 6 neurons, 3 mice). Left: $NI_{\text{before}} = -1.7\% \pm 1.7\%$, $p = 0.91$; $NI_{\text{after}} = 18.4\% \pm 2.6\%$, $p = 0.0021$. Right, NI_{before} versus NI_{after} , $p = 0.000059$. NI_{before} , $p = 0.0094$; NI_{after} , $p = 0.25$.
- (K) No spermine, 10 ms ($n = 14$, 9 neurons, 4 mice). Left: $NI_{\text{before}} = -2.6\% \pm 2.9\%$, $p = 0.16$; $NI_{\text{after}} = 13.7\% \pm 3.7\%$, $p = 0.047$. Right: NI_{before} versus NI_{after} , $p = 0.0012$. NI_{before} , $p = 0.031$; NI_{after} , $p = 0.19$.
- t tests were run unless otherwise specified.

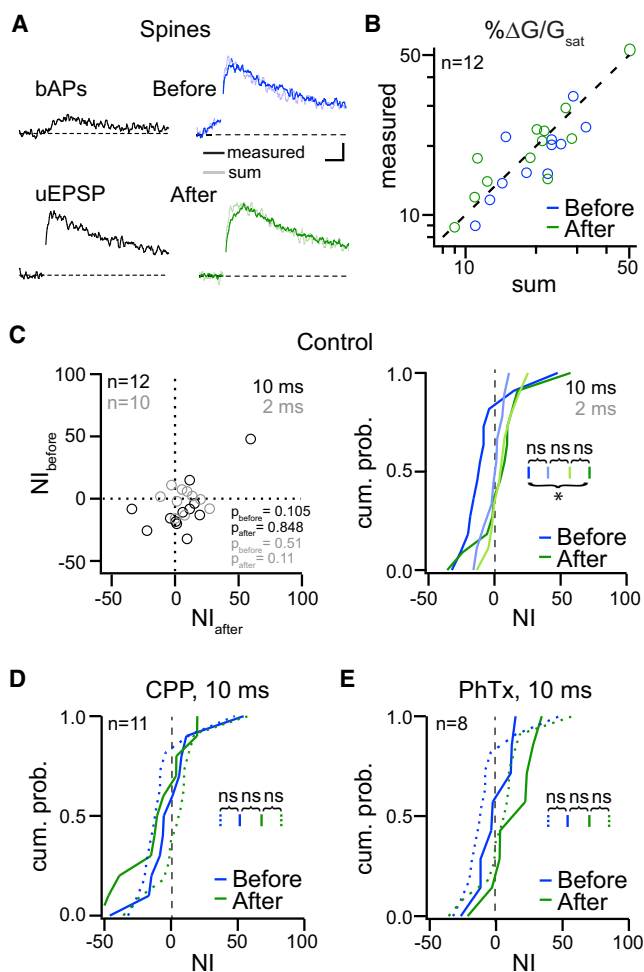


Figure 6. Spine CP-AMPA and NMDARs Do Not Exhibit Modulation by Somatic Activity

(A) Average Ca transients measured from the spine in response to 5 bAPs (3.8 ± 1.4) or glutamate uncaging alone (18.4 ± 2.4) and in the before (21.6 ± 3.5) and after (21.3 ± 3.2) pairing configurations. Scale bars, 5% $\Delta G/G_{sat}$ and 50 ms. (B) Measured versus sum of the Ca transients produced by bAPs and uEPSP alone ($n = 12$, 10 neurons, 6 mice).

(C) Control, 10 ms (black) and 2 ms (gray). Left: NIs for each spine (10 ms: $n = 12$, 10 neurons, 6 mice; 2 ms: $n = 10$, 7 neurons, 4 mice). 10 ms: $NI_{before} = -7.9\% \pm 6.1\%$ ($p = 0.11$), $NI_{after} = 4.3\% \pm 6.6\%$ ($p = 0.85$); 2 ms: $NI_{before} = -1.3\% \pm 2.8\%$ ($p = 0.51$), $NI_{after} = 5.1\% \pm 3.6\%$ ($p = 0.11$; measured versus sum). Right: cumulative probability distributions of the NIs. 10 ms: NI_{before} versus NI_{after} , $p = 0.032$; 2 ms: $p = 0.24$. 10 ms versus 2 ms: NI_{before} , $p = 0.065$. NI_{after} , $p = 0.90$.

(D and E) Between-condition comparisons done against control, 10 ms data (dotted lines). (D) Cumulative probability distributions of the NIs as in (C), but in CPP ($n = 11$, 7 neurons, 4 mice). $NI_{before} = -1.5\% \pm 7.3\%$, $p = 0.51$. $NI_{after} = -12.4\% \pm 7.5\%$, $p = 0.11$. (E) Cumulative probability distributions of the NIs as in (C), but in PhTx ($n = 8$, 6 neurons, 2 mice). $NI_{before} = -2.4\% \pm 5.1\%$, $p = 0.49$. $NI_{after} = 11.0\% \pm 6.7\%$, $p = 0.48$. t tests were run.

function within a circuit. Selective deletion of NMDARs in PV INs leads to the dysregulation of gamma oscillations in the cortex, reduction of the spatial coherence of place cells in the hippocampus, and a host of behavioral abnormalities (Carlén et al.,

2012; Korotkova et al., 2010; Cardin et al., 2009). Indeed, NMDAR hypofunction is a leading hypothesis for the etiology of schizophrenia. Despite the low expression levels of NMDARs in PV INs, these receptors are critical for dynamic synaptic responses to different kinds of cellular activity. Deeper understanding of the distinct functions of NMDARs at spine and dendritic synapses will provide insight into PV IN function in healthy states and dysfunction in psychiatric disorders.

EXPERIMENTAL PROCEDURES

Animal Use and Handling

Animals were handled according to protocols approved by the UC San Diego Institutional Animal Care and Use Committee (IACUC) and were in accordance with NIH guidelines. Male and female *Pvalb^{tm1(cre)Arbr} × Gt(ROSA)26Sor^{tm14(CAG-tdTomato)Hze}* mice in a C57B/6 background (Jackson Laboratories, *Pvalb^{tm1(cre)Arbr}*: 008069, *Gt(ROSA)26Sor^{tm14(CAG-tdTomato)Hze}*: 007914) were used. Mice were housed in a standard, temperature-controlled vivarium on a 12 hr:12 hr light/dark cycle and received water and food *ad libitum*. For a subset of experiments ($n = 2-4$ for each condition in Figures 3 and 4), wild-type C57B/6 mice were used and fast-spiking INs were identified by morphology and electrophysiology. All experiments were performed on P15–P19 mice, except for spine density quantification, which was performed in mice up to P56.

Immunostaining and Confocal Imaging

A *Pvalb^{tm1(cre)Arbr} × Gt(ROSA)26Sor^{tm14(CAG-tdTomato)Hze}* mouse (P25) was perfused and 100 μm coronal sections cut using a Leica VT1000s vibratome. Sections were immunostained with rabbit anti-RFP (Abcam, ab62341) and imaged by confocal microscopy. See Supplemental Experimental Procedures for the perfusion and staining protocol used.

Acute Slice Preparation

Sagittal slices (300 μm) from V1 were prepared from mice as described in Xue et al. (2014). See Supplemental Experimental Procedures for details.

Spine Quantification

Whole-cell recordings were made from PV INs, cells were filled with 100 μM Alexa Fluor-594, and morphology was visualized under two-photon microscopy using 800-nm light. Images were stitched together using an ImageJ pairwise Stitching plugin (Preibisch et al., 2009), and spines were manually counted.

Electrophysiology

tdTomato-expressing INs in layer II/III of V1 were visualized using epifluorescence, and targeted recordings were made under infrared differential interference contrast (IR-DIC) on an Olympus BX51 microscope. Whole-cell patch-clamp recordings were performed using a Multiclamp 700B amplifier (Molecular Devices, Sunnyvale, CA). For all Ca imaging experiments, neurons were filled with the Ca-sensitive green fluorophore Fluo-5F (300 μM) and Ca-insensitive red fluorophore Alexa Fluor-594 (15 μM). Spermine (100 μM) was included in the intracellular solution unless stated otherwise. For voltage-clamp experiments, neurons were held at -70 mV. For current-clamp experiments, a resting membrane potential of approximately -70 mV was maintained by current injection (approximately <150 pA). See Supplemental Experimental Procedures for details.

EC Stimulation Experiments

Synaptic currents were evoked with a theta-glass stimulating electrode placed 10–15 μm away from a spine or dendrite as described in Goldberg et al. (2003a). EPSCs were recorded at the soma, and Ca transients were measured in the region of interest. For details, see Supplemental Experimental Procedures.

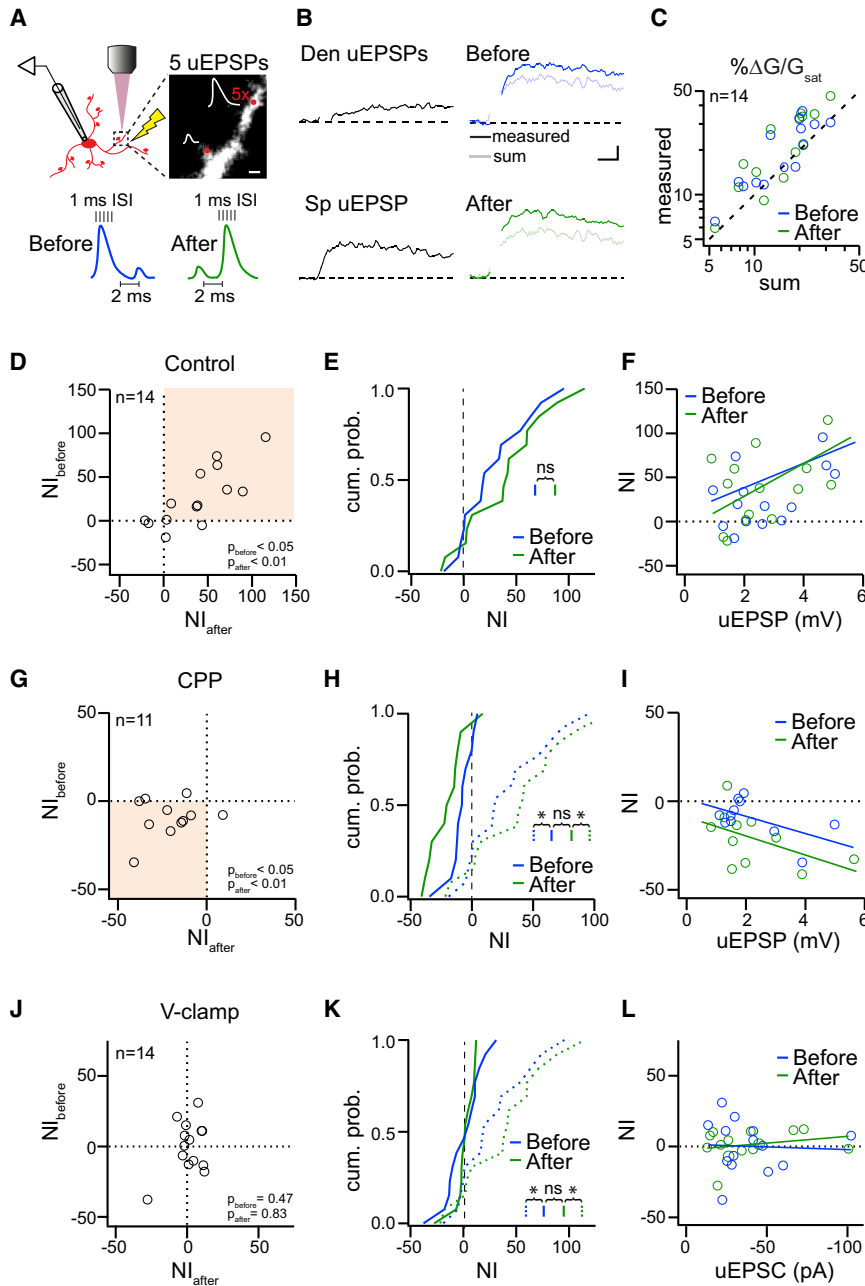


Figure 7. Spines on PV INs Produce NMDAR-Dependent Supra-linear Ca Signals in Response to Local Dendritic Activity

(A) Schematic depicting 5 dendritic uEPSPs (at 100 Hz; 10–15 μm away) either 2 ms before or after a spine uEPSP. Scale bar, 1 μm .

(B) Average Ca transients from different paradigms: spine uEPSPs only (“Sp uEPSP”; 13.5 ± 1.6), dendritic uEPSPs only (“Den uEPSP”; 3.8 ± 0.6), before (20.7 ± 2.6), and after (22.9 ± 3.2). Scale bars, 5% $\Delta\text{G}/\text{G}_{\text{sat}}$ and 25 ms.

(C) Measured versus sum of the Ca transients produced by bAPs and uEPSP alone ($n = 14$, 10 neurons, 6 mice).

(D) NIs for each spine ($n = 14$, 10 neurons, 6 mice). $\text{NI}_{\text{before}} = 27.3\% \pm 9.0\%$, $p = 0.022$; $\text{NI}_{\text{after}} = 37.7\% \pm 10.7\%$, $p = 0.0033$ (measured versus sum).

(E) Control, cumulative probability distributions of the NIs. $\text{NI}_{\text{before}}$ versus NI_{after} , $p = 0.14$.

(F) NI versus peak uEPSP. Before: slope = 12.8 ± 6.2 , $r^2 = 0.262$; after: slope = 12.3 ± 7.9 , $r^2 = 0.167$.

(G) As in (D), but for CPP ($n = 11$, 6 neurons, 4 mice). $\text{NI}_{\text{before}} = -9.4\% \pm 3.2\%$, $p = 0.012$; $\text{NI}_{\text{after}} = -21.0\% \pm 1.6\%$, $p = 0.0080$.

(H) Cumulative probability distributions of the NIs as in (E), but in CPP. $\text{NI}_{\text{before}}$ versus NI_{after} , $p = 0.12$. Dotted lines: control in (E). $\text{NI}_{\text{before}}$, $p = 0.014$; NI_{after} , $p = 0.00086$ (CPP versus control).

(I) NI versus peak uEPSP. Before: slope = -4.8 ± 2.4 , $r^2 = -0.309$; after: slope = -5.4 ± 3.1 , $r^2 = -0.255$.

(J) As in (D), but for the voltage (V)-clamp condition ($n = 14$, 8 neurons, 5 mice). $\text{NI}_{\text{before}} = 0.18\% \pm 6.0\%$, $p = 0.47$; $\text{NI}_{\text{after}} = 1.2\% \pm 3.4\%$, $p = 0.83$.

(K) As in (E), but in V-clamp. $\text{NI}_{\text{before}}$ versus NI_{after} , $p = 0.88$. $\text{NI}_{\text{before}}$, $p = 0.015$; NI_{after} , $p = 0.0050$ (V-clamp versus current [I]-clamp).

(L) NI versus peak uEPSC. Before: slope = 0.038 ± 0.23 , $r^2 = 0.0022$; after: slope = -0.096 ± 0.11 , $r^2 = 0.057$. t tests were run.

Pharmacology

Pharmacology was used as indicated in the text with final concentrations of 10 μM CPP (#0247, Tocris, Ellisville, MO), 10 μM NBQX (#1044, Tocris, Ellisville, MO), 10 μM PhTx-433 (sc-255421, Santa Cruz Biotechnology, Dallas, TX), 0.2 μM TTX (tetrodotoxin citrate; ab120055, Abcam, Cambridge, UK), and 50 μM picrotoxin (#1128, Tocris). All agents were dissolved in double distilled water and added to the artificial cerebrospinal fluid (aCSF) on the day of the experiment. First ~ 10 trials after wash-in or use were excluded.

Two-Photon Imaging and Uncaging

Combined two-photon imaging and MNI-glutamate uncaging was performed using a custom-built two-photon laser-scanning microscope (as

described in Bloodgood and Sabatini, 2007; Carter and Sabatini, 2004). Uncaging laser power was set to bleach 30%–40% of the red fluorescence across all conditions (Bloodgood and Sabatini, 2007; Figures S2A–S2C and S2F; Supplemental Experimental Procedures). For probing synapses formed directly on the dendritic shaft, the laser power was set by photobleaching a neighboring spine located within the same z-plane. All experiments were performed using ScanImage software (Pologruto et al., 2003). Uncaging produced uEPSCs that were similar in amplitude and rise times to miniature EPSCs (mEPSCs) recorded in these cells (Figures S2D and S2E; Supplemental Experimental Procedures).

Data Analysis

Offline data analyses were performed using custom software in Igor Pro (WaveMetrics) and MATLAB. Briefly, trials were averaged, baselined to the period immediately preceding the stimulus, and smoothed. The RI (Figures 4F and S3) was calculated as previously described (Soto et al., 2007), and the NIs (Figures 5, 6, and 7) as the difference between the sum and the experimental pairing was divided by the experimental pairing and multiplied by 100.

Statistics

Datasets were tested for normality and appropriate statistical tests were conducted using IBM SPSS; specific tests used are noted in the figure legends. In all cases, significance was set at $p < 0.05$.

SUPPLEMENTAL INFORMATION

Supplemental Information includes Supplemental Experimental Procedures and six figures and can be found with this article online at <https://doi.org/10.1016/j.celrep.2018.07.070>.

ACKNOWLEDGMENTS

This work was supported by grants from the Pew Charitable Trust (00028631), the Searle Scholars Program (14-SSP-184), and the Whitehall Foundation (2013-12-88). The authors would like to thank M. Banghart and J. Isaacson and the members of the lab for critical reading of the manuscript and insightful feedback.

AUTHOR CONTRIBUTIONS

Conceptualization, Methodology, Writing, and Visualization, L.S. and B.L.B.; Formal Analysis and Investigation, L.S.; Supervision and Funding Acquisition, B.L.B.

DECLARATION OF INTERESTS

The authors declare no competing interests.

Received: March 15, 2018

Revised: June 15, 2018

Accepted: July 19, 2018

Published: August 21, 2018

REFERENCES

- Araya, R., Eisenthal, K.B., and Yuste, R. (2006). Dendritic spines linearize the summation of excitatory potentials. *Proc. Natl. Acad. Sci. USA* *103*, 18799–18804.
- Azouz, R., Gray, C.M., Nowak, L.G., and McCormick, D.A. (1997). Physiological properties of inhibitory interneurons in cat striate cortex. *Cereb. Cortex* *7*, 534–545.
- Bagnall, M.W., Hull, C., Bushong, E.A., Ellisman, M.H., and Scanziani, M. (2011). Multiple clusters of release sites formed by individual thalamic afferents onto cortical interneurons ensure reliable transmission. *Neuron* *71*, 180–194.
- Bloodgood, B.L., and Sabatini, B.L. (2007). Nonlinear regulation of unitary synaptic signals by CaV(2.3) voltage-sensitive calcium channels located in dendritic spines. *Neuron* *53*, 249–260.
- Bloodgood, B.L., and Sabatini, B.L. (2009). NMDA receptor-mediated calcium transients in dendritic spines. In *Biology of the NMDA Receptor*, A.M. Van Dongen, ed. (CRC Press/Taylor & Francis), pp. 201–211.
- Bloodgood, B.L., Giessel, A.J., and Sabatini, B.L. (2009). Biphasic synaptic Ca influx arising from compartmentalized electrical signals in dendritic spines. *PLoS Biol.* *7*, e1000190.
- Bowie, D., and Mayer, M.L. (1995). Inward rectification of both AMPA and kainate subtype glutamate receptors generated by polyamine-mediated ion channel block. *Neuron* *15*, 453–462.
- Branco, T., and Häusser, M. (2011). Synaptic integration gradients in single cortical pyramidal cell dendrites. *Neuron* *69*, 885–892.
- Camiré, O., and Topolnik, L. (2014). Dendritic calcium nonlinearities switch the direction of synaptic plasticity in fast-spiking interneurons. *J. Neurosci.* *34*, 3864–3877.
- Cardin, J.A., Carlén, M., Meletis, K., Knoblich, U., Zhang, F., Deisseroth, K., Tsai, L.H., and Moore, C.I. (2009). Driving fast-spiking cells induces gamma rhythm and controls sensory responses. *Nature* *459*, 663–667.
- Carlén, M., Meletis, K., Siegle, J.H., Cardin, J.A., Futai, K., Vierling-Claassen, D., Rühlmann, C., Jones, S.R., Deisseroth, K., Sheng, M., et al. (2012). A critical role for NMDA receptors in parvalbumin interneurons for gamma rhythm induction and behavior. *Mol. Psychiatry* *17*, 537–548.
- Carter, A.G., and Sabatini, B.L. (2004). State-dependent calcium signaling in dendritic spines of striatal medium spiny neurons. *Neuron* *44*, 483–493.
- Colgan, L.A., and Yasuda, R. (2014). Plasticity of dendritic spines: subcompartmentalization of signaling. *Annu. Rev. Physiol.* *76*, 365–385.
- Froemke, R.C., and Dan, Y. (2002). Spike-timing-dependent synaptic modification induced by natural spike trains. *Nature* *416*, 433–438.
- Geiger, J.R., Melcher, T., Koh, D.S., Sakmann, B., Seeburg, P.H., Jonas, P., and Monyer, H. (1995). Relative abundance of subunit mRNAs determines gating and Ca²⁺ permeability of AMPA receptors in principal neurons and interneurons in rat CNS. *Neuron* *15*, 193–204.
- Geiger, J.R.P., Lübke, J., Roth, A., Frotscher, M., and Jonas, P. (1997). Submillisecond AMPA receptor-mediated signaling at a principal neuron-interneuron synapse. *Neuron* *18*, 1009–1023.
- Gilbert-Juan, J., Castillo-Gomez, E., Pérez-Rando, M., Moltó, M.D., and Nacher, J. (2011). Chronic stress induces changes in the structure of interneurons and in the expression of molecules related to neuronal structural plasticity and inhibitory neurotransmission in the amygdala of adult mice. *Exp. Neurol.* *232*, 33–40.
- Goldberg, J.H., Tamas, G., Aronov, D., and Yuste, R. (2003a). Calcium microdomains in aspiny dendrites. *Neuron* *40*, 807–821.
- Goldberg, J.H., Tamas, G., and Yuste, R. (2003b). Ca²⁺ imaging of mouse neocortical interneurone dendrites: Ia-type K⁺ channels control action potential backpropagation. *J. Physiol.* *551*, 49–65.
- Goldberg, J.H., Yuste, R., and Tamas, G. (2003c). Ca²⁺ imaging of mouse neocortical interneurone dendrites: contribution of Ca²⁺-permeable AMPA and NMDA receptors to subthreshold Ca²⁺ dynamics. *J. Physiol.* *551*, 67–78.
- Guirado, R., Perez-Rando, M., Sanchez-Matarredona, D., Castillo-Gómez, E., Liberia, T., Rovira-Esteban, L., Varela, E., Crespo, C., Blasco-Ibáñez, J.M., and Nacher, J. (2014). The dendritic spines of interneurons are dynamic structures influenced by PSA-NCAM expression. *Cereb. Cortex* *24*, 3014–3024.
- Gulledge, A.T., Carnevale, N.T., and Stuart, G.J. (2012). Electrical advantages of dendritic spines. *PLoS ONE* *7*, e36007.
- Gulyás, A.I., Megiás, M., Emri, Z., and Freund, T.F. (1999). Total number and ratio of excitatory and inhibitory synapses converging onto single interneurons of different types in the CA1 area of the rat hippocampus. *J. Neurosci.* *19*, 10082–10097.
- Hu, H., Martina, M., and Jonas, P. (2010). Dendritic mechanisms underlying rapid synaptic activation of fast-spiking hippocampal interneurons. *Science* *327*, 52–58.
- Jayant, K., Hirtz, J.J., Plante, I.J., Tsai, D.M., De Boer, W.D.A.M., Semonche, A., Peterka, D.S., Owen, J.S., Sahin, O., Shepard, K.L., and Yuste, R. (2017). Targeted intracellular voltage recordings from dendritic spines using quantum-dot-coated nanopipettes. *Nat. Nanotechnol.* *12*, 335–342.
- Jonas, P., Racca, C., Sakmann, B., Seeburg, P.H., and Monyer, H. (1994). Differences in Ca²⁺ permeability of AMPA-type glutamate receptor channels in neocortical neurons caused by differential GluR-B subunit expression. *Neuron* *12*, 1281–1289.
- Kamboj, S.K., Swanson, G.T., and Cull-Candy, S.G. (1995). Intracellular spermine confers rectification on rat calcium-permeable AMPA and kainate receptors. *J. Physiol.* *486*, 297–303.
- Kawaguchi, Y., Karube, F., and Kubota, Y. (2006). Dendritic branch typing and spine expression patterns in cortical nonpyramidal cells. *Cereb. Cortex* *16*, 696–711.
- Kawato, M., and Tsukahara, N. (1984). Electrical properties of dendritic spines with bulbous end terminals. *Biophys. J.* *46*, 155–166.
- Keck, T., Scheuss, V., Jacobsen, R.I., Wierenga, C.J., Eysel, U.T., Bonhoeffer, T., and Hübener, M. (2011). Loss of sensory input causes rapid structural changes of inhibitory neurons in adult mouse visual cortex. *Neuron* *71*, 869–882.

- Kloc, M., and Maffei, A. (2014). Target-specific properties of thalamocortical synapses onto layer 4 of mouse primary visual cortex. *J. Neurosci.* *34*, 15455–15465.
- Korotkova, T., Fuchs, E.C., Ponomarenko, A., von Engelhardt, J., and Monyer, H. (2010). NMDA receptor ablation on parvalbumin-positive interneurons impairs hippocampal synchrony, spatial representations, and working memory. *Neuron* *68*, 557–569.
- Kubota, Y., Karube, F., Nomura, M., Gullledge, A.T., Mochizuki, A., Schertel, A., and Kawaguchi, Y. (2011). Conserved properties of dendritic trees in four cortical interneuron subtypes. *Sci. Rep.* *1*, 89.
- Kwon, T., Sakamoto, M., Peterka, D.S., and Yuste, R. (2017). Attenuation of synaptic potentials in dendritic spines. *Cell Rep.* *20*, 1100–1110.
- Lamsa, K.P., Heeroma, J.H., Somogyi, P., Rusakov, D.A., and Kullmann, D.M. (2007). Anti-Hebbian long-term potentiation in the hippocampal feedback inhibitory circuit. *Science* *315*, 1262–1266.
- Le Roux, N., Cabezas, C., Böhm, U.L., and Poncer, J.C. (2013). Input-specific learning rules at excitatory synapses onto hippocampal parvalbumin-expressing interneurons. *J. Physiol.* *591*, 1809–1822.
- Lee, K.F.H., Soares, C., Thivierge, J.P., and Béique, J.C. (2016). Correlated synaptic inputs drive dendritic calcium amplification and cooperative plasticity during clustered synapse development. *Neuron* *89*, 784–799.
- Lester, R.A.J., Clements, J.D., Westbrook, G.L., and Jahr, C.E. (1990). Channel kinetics determine the time course of NMDA receptor-mediated synaptic currents. *Nature* *346*, 565–567.
- Losonczy, A., and Magee, J.C. (2006). Integrative properties of radial oblique dendrites in hippocampal CA1 pyramidal neurons. *Neuron* *50*, 291–307.
- Magee, J.C., and Johnston, D. (1997). A synaptically controlled, associative signal for Hebbian plasticity in hippocampal neurons. *Science* *275*, 209–213.
- Markram, H., Lubke, J., Frotscher, M., and Sakmann, B. (1997). Regulation of synaptic efficacy by coincidence of postsynaptic APs and EPSPs. *Science* *275*, 213–215.
- Matta, J.A., Pelkey, K.A., Craig, M.T., Chittajallu, R., Jeffries, B.W., and McBain, C.J. (2013). Developmental origin dictates interneuron AMPA and NMDA receptor subunit composition and plasticity. *Nat. Neurosci.* *16*, 1032–1041.
- Monyer, H., Sprengel, R., Schoepfer, R., Herb, A., Higuchi, M., Lomeli, H., Burnashev, N., Sakmann, B., and Seeburg, P.H. (1992). Heteromeric NMDA receptors: molecular and functional distinction of subtypes. *Science* *256*, 1217–1221.
- Murakoshi, H., Wang, H., and Yasuda, R. (2011). Local, persistent activation of Rho GTPases during plasticity of single dendritic spines. *Nature* *472*, 100–104.
- Nevian, T., and Sakmann, B. (2006). Spine Ca²⁺ signaling in spike-timing-dependent plasticity. *J. Neurosci.* *26*, 11001–11013.
- Nishiyama, J., and Yasuda, R. (2015). Biochemical computation for spine structural plasticity. *Neuron* *87*, 63–75.
- Nissen, W., Szabo, A., Somogyi, J., Somogyi, P., and Lamsa, K.P. (2010). Cell type-specific long-term plasticity at glutamatergic synapses onto hippocampal interneurons expressing either parvalbumin or CB1 cannabinoid receptor. *J. Neurosci.* *30*, 1337–1347.
- Nowak, L., Bregestovski, P., Ascher, P., Herbet, A., and Prochiantz, A. (1984). Magnesium gates glutamate-activated channels in mouse central neurones. *Nature* *307*, 462–465.
- Pelkey, K.A., Barksdale, E., Craig, M.T., Yuan, X., Sukumaran, M., Vargish, G.A., Mitchell, R.M., Wyeth, M.S., Petralia, R.S., Chittajallu, R., et al. (2015). Pentraxins coordinate excitatory synapse maturation and circuit integration of parvalbumin interneurons. *Neuron* *85*, 1257–1272.
- Pérez-Rando, M., Castillo-Gómez, E., Bellés, M., Carceller, H., and Nácher, J. (2017). The activation of NMDA receptors alters the structural dynamics of the spines of hippocampal interneurons. *Neurosci. Lett.* *658*, 79–84.
- Peters, A., and Regidor, J. (1981). A reassessment of the forms of nonpyramidal neurons in area 17 of cat visual cortex. *J. Comp. Neurol.* *203*, 685–716.
- Pologruto, T.A., Sabatini, B.L., and Svoboda, K. (2003). ScanImage: flexible software for operating laser scanning microscopes. *Biomed. Eng. Online* *2*, 13.
- Preibisch, S., Saalfeld, S., and Tomancak, P. (2009). Globally optimal stitching of tiled 3D microscopic image acquisitions. *Bioinformatics* *25*, 1463–1465.
- Sabatini, B.L., and Svoboda, K. (2000). Analysis of calcium channels in single spines using optical fluctuation analysis. *Nature* *408*, 589–593.
- Sobczyk, A., Scheuss, V., and Svoboda, K. (2005). NMDA receptor subunit-dependent [Ca²⁺] signaling in individual hippocampal dendritic spines. *J. Neurosci.* *25*, 6037–6046.
- Soto, D., Coombs, I.D., Kelly, L., Farrant, M., and Cull-Candy, S.G. (2007). Stargazin attenuates intracellular polyamine block of calcium-permeable AMPA receptors. *Nat. Neurosci.* *10*, 1260–1267.
- Szabo, A., Somogyi, J., Cauli, B., Lambomez, B., Somogyi, P., and Lamsa, K.P. (2012). Calcium-permeable AMPA receptors provide a common mechanism for LTP in glutamatergic synapses of distinct hippocampal interneuron types. *J. Neurosci.* *32*, 6511–6516.
- Washburn, M.S., Numberger, M., Zhang, S., and Dingledine, R. (1997). Differential dependence on GluR2 expression of three characteristic features of AMPA receptors. *J. Neurosci.* *17*, 9393–9406.
- Xue, M., Atallah, B.V., and Scanziani, M. (2014). Equalizing excitation-inhibition ratios across visual cortical neurons. *Nature* *511*, 596–600.
- Yuste, R. (2013). Electrical compartmentalization in dendritic spines. *Annu. Rev. Neurosci.* *36*, 429–449.
- Yuste, R., and Denk, W. (1995). Dendritic spines as basic functional units of neuronal integration. *Nature* *375*, 682–684.